High-Performance Tunable Multichannel Absorbers Coupled with Graphene-Based Grating and Dual-Tamm Plasmonic Structures

Jinlei Hu[1] · Zhengda Hu[1] · Jicheng Wang[1,2] · Aliaksei Balmakou[3] · Sergei Khakhomov[3] · Igor Semchenko[3]

Abstract

We present a hybrid Tamm system targeting the tunable multichannel absorber. The proposed optical absorber is analyzed and investigated by using the transfer matrix method (TMM). The numerical and theoretical studies show that the four perfect absorption peaks are generated by two types of resonant modes excited in the structure, which can be reasonably explained by the guided-mode resonance (GMR) and optical Tamm state (OTS). More importantly, the strong interaction between the two modes gives rise to mode hybridization by adjusting the grating period. Furthermore, the active modulation of the GMR-based peak can be manipulated discretely by tuning the polarization angle or continuously by changing the chemical potential of graphene. The presented optical absorption filter will meet high level of effectiveness in developing high-performance optoelectronic devices.

Introduction

In recent years, there has been an increased interest in a special type of surface electromagnetic states called the optical Tamm states (OTSs) because of their potential applications in narrow-bandwidth multichannel absorbers and thermal emission devices [1–3]. These states are analogous to the Tamm states in condensed matter physics. The first proposed OTS is excited between two photonic crystals (PhCs) [4]. Subsequently, the OTS generated near the interface between metal and photonic crystal is proposed, which is also called Tamm plasmon polariton (TPP) [5, 6]. The PhC is a special structure produced by the periodic stacking of high refractive index materials [7] and low refractive index materials. And the common Bragg reflector (BR) is a simple one-dimensional PhC in optics [5, 13]. The two materials in the BR need to have a good light transmission in the considered waveband and the specific lattice structure periodicity [8, 9]. Compared with traditional surface states such as surface plasmon polarization (SPP) [10–12], TPP modes could be excited with either TE or TM polarization [13, 14] without requiring a specific incident angle [15–17].

The plasmonic reaction of graphene and the applications of the Tamm structure have attracted widespread attention [18–22]. Plasmonic reaction, which occurs in many semiconductors and metals, is ubiquitous, high-frequency, collective density oscillations of an electron liquid [19]. Graphene, an attractive, atomically thin carbon material that can replace metals, has shown a plasmonic reaction in the infrared region, featuring greatly enhanced electric field and ultra-fast optical tunability [19, 20]. Surface plasmons (SPs) in graphene are electromagnetic waves that propagate along the surface of the graphene due to the infrared light-induced oscillation of surface charges, which can effectively enhance optical absorption [20–22]. In order to better improve the light absorption performance of the graphene monolayer, a simple method of guided-mode resonance (GMR) can be introduced to maintain SPs [23–25]. It is difficult to realize TPP in practice because the photonic local field of the Tamm plasmon is near the interface between the metal film and the photonic crystal, that is, inside the Tamm structure.

✉ Jicheng Wang
  jcwang@jiangnan.edu.cn

1 School of Science, Jiangsu Provincial Research Center of Light Industrial Optoelectronic Engineering and Technology, Jiangnan University, Wuxi 214122, China

2 State Key Laboratory of Applied Optics, Fine Mechanics and Physics, Changchun Institute of Optics, Chinese Academy of Sciences, Changchun 130033, China

3 Departments of Optics, Francisk Skorina Gomel State University, 246019 Gomel, Belarus

There are currently three research techniques to make the idea workable: adjusting the structure of the photonic crystal, changing the structure of the metal layer, or using the coupling of the Tamm structure with other structures to distribute the photonic local field in an appropriate position. Wurdack et al. [27] utilized organic materials to connect metal thin films and photonic crystals, then embedded single-layer tungsten diselenide films [26] and single-layer molybdenum diselenide films [27] into the connection materials. The organic material has a refractive index similar to that of the low refractive index material in the photonic crystal. Mischok et al. [28] investigated a metal–organic-metal microcavity structure to replace the metal layer in the Tamm structure, and realized the regulation of the Tamm plasmon by changing the organic layer. Maji and Das [29] and Kumar et al. [30] numerically determined two reverse Tamm structures to add materials to be detected in the metal cavity, facilitating the design of a temperature sensor [29] and a refractive index sensor [30].
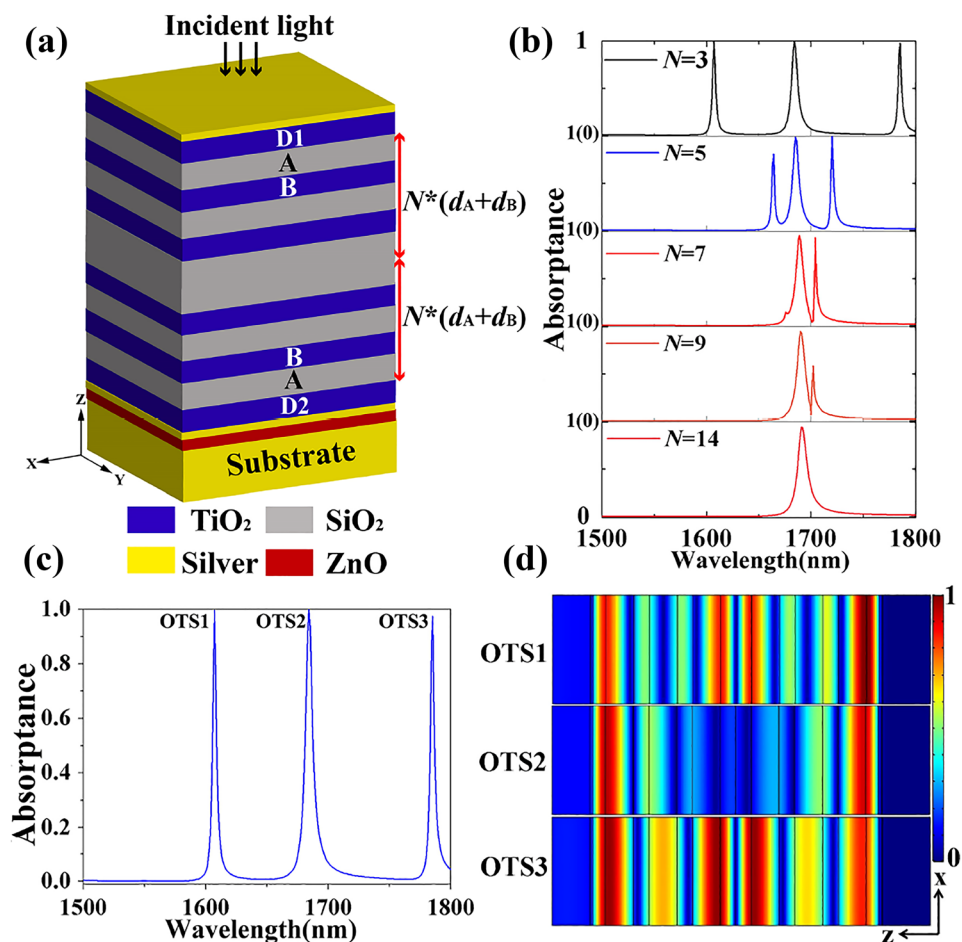
In this paper, we propose to achieve high-performance tunable multichannel absorption filters based on the grating layer and metal-photonic crystal heterostructure-metal (M-PCH-M). The GMR and TPP resonances can be excited simultaneously at near-infrared frequencies. The simulation results show that the three high-efficiency TPP peaks can be maintained by adjusting the thickness of thin silver films and the top layer thickness in the M-PCH-M. Furthermore, the strong coupling between the two modes gives rise to mode hybridization. Transfer matrix theory (TMT) has been employed to explain the strong coupling phenomenon. To investigate the optical properties in this hybrid structure, simulations are achieved by using the finite element method. In addition, the modulation of GMR-based absorption can be actively controlled by adjusting the polarization angle or chemical potential of graphene. The proposed optical multichannel absorption filter has potential applications in modulators, solar cells, sensors, and thermal radiation.

Structure and Theory

In Fig. 1a, we demonstrate a part of the hybrid Tamm structure, in which the M-PCH-M structure is deposited on a ZnO film and a thick silver layer substrate. The x and y directions of the structure are infinitely extended. In the COMSOL simulation, in order to simplify the calculation, we only

Fig.1 **a** Schematic diagram of the structure composed of upper silver film/PCH/lower silver film/ZnO/silver substrate. **b** The two side peaks can be eliminated by increasing the number of layers N of the dual PhCs. **c** The three perfect absorption peaks were realized for the depicted structure when $N = 3$. **d** The electric field distributions for the three peaks corresponding to TPP modes: OTS1, OTS2, OTS3

simulate the modeling of the x–z section and the y direction is infinitely wide by default. Periodic boundary conditions are set on both sides of the structure in the x direction, and perfectly matched layers are added up and down to absorb the outgoing light. By using periodic boundary conditions, the simulation of complex structures can be simplified into periodic elements to improve convergence. Meeting the phase-matching condition [35, 36] in Eq. (11), a plane wave of TM polarization (i.e., electric field has no component in the y direction) or TE polarization (i.e., the electric field has a component in the y direction) is injected onto the structure at an angle of θ to excite the TPP mode at the interface between the PhC and thin silver layer. The thickness of the ZnO layer in the structure is 12 nm, and the upper and lower layers in the M-PCH-M structure are thin sliver films, with the thickness of $t_m = 27$ nm. The silver substrate with a thickness much larger than the penetration depth of the incident radiation is added under the structure to block all transmission. The dielectric constant of silver can be characterized by the Drude model [31]:

$$\varepsilon_r = \varepsilon_\infty - \frac{\omega_p^2}{\omega^2 + i\omega\gamma} - \frac{\Delta \times \Omega^2}{(\omega^2 - \Omega^2) + i\Gamma} \tag{1}$$

where $\varepsilon_\infty = 2.4064$ is the dielectric constant when the frequency of the incident light ω tends to infinity, $\gamma = 2\pi \times 4.8 \times 10^{12}$ Hz is the collision frequency, $\omega_p = 2\pi \times 2214.6 \times 10^{12}$ Hz is the plasmon frequency, $\Delta = 1.6604$ is the weight coefficient of Lorentz item, $\Omega = 2\pi \times 620.7 \times 10^{12}$ Hz is the strength of Lorentz harmonic oscillator, and $\Gamma = 2\pi \times 1330.1 \times 10^{12}$ Hz is the spectral width of vibration.

In the simulated structure, the PhC is composed of alternating layers of silicon dioxide (SiO_2) and titanium dioxide (TiO_2). As a one-dimensional photonic crystal, the BR is a reflector used in a waveguide. When light passes through different media, it will be reflected at the interface, and the reflectivity will be related to the refractive index between the media [5, 13]. Here, the refractive indices of SiO_2 and TiO_2 are $n_A = 1.45$ and $n_B = 2.6$, respectively. The conditions of Bragg incident light are met by selecting the thickness of the SiO_2 and TiO_2 layers: $d_A = \lambda_M/4n_A$ and $d_B = \lambda_M/4n_B$, where λ_M is the central resonant wavelength of BR. The number of periodic layers of PhCs is both N. In order to effectively excite the OTSs, a material with a higher refractive index should be incorporated as the top layer. The relevant material of the top layer D1 and lower layer D2 is determined to be TiO_2, with their thickness to be optimized at $D = 136$ nm.

With the increase of the number of periodic layers N of the dual PhCs, the Tamm absorption peaks of the structure gradually change as shown in Fig. 1b. When the number N of the dual PhCs increases from 3 to 14 pairs continuously, the side TPP peaks gradually move inside just to finally merge into a single peak. Figure 1c is the absorptance spectrum of the designed structure being excited by the TE polarization when incident normally when $N = 3$. It can be seen from Fig. 3c that the electric field enhancement with wavelengths of 1607 nm and 1785 nm are mainly distributed at the interface of dual PhCs and M-PhC. And the electric field enhancement with the wavelength of 1684 nm is mainly concentrated on the two interfaces of M-PhC and PhC-M.

The transmission characteristics of the M-PCH-M part of the structure can be analyzed by the TMM:

$$E_{out} = ME_{in} \tag{2}$$

where E_{out} and E_{in} are the electric fields of output light and incident light, respectively, and M is the transfer matrix of light in the structure, which can be expressed as follows:

$$M = \begin{bmatrix} M_{11} & M_{12} \\ M_{21} & M_{22} \end{bmatrix} = m_{Ag}m_{D1}(m_Am_B)^N(m_Bm_A)^Nm_{D2}m_{Ag} \tag{3}$$

where, m_{Ag}, m_{D1}, m_A, m_B, and m_{D2} represent the transmission matrix of light through each layer, and N is the number of periodic layers of the two photonic crystals.

The TMM of incident light in each layer can be expressed as:

$$m_i = \begin{bmatrix} \cos\delta_i & -ip_i^{-1}\sin\delta_i \\ -ip_i\sin\delta_i & \cos\delta_i \end{bmatrix} \tag{4}$$

In formula 4, $\delta_i = (2\pi/\lambda)n_id_i\cos\theta_i$, where n_id_i is the optical thickness of the corresponding layer, θ_i is the angle between the light in the dielectric layer and the normal direction of the interface, and λ is the wavelength of incident light. When the incident light is incident with TM or TE polarization, the corresponding p_i has the following formulas:

$$P_i = \sqrt{\varepsilon_0\mu_0n_i}/\cos\theta_i \tag{5}$$

$$P_i = \sqrt{\varepsilon_0/\mu_0}n_i\cos\theta_i \tag{6}$$

where $i = m_{Ag}$, m_D, m_{SiO2}, or m_{TiO2}, then ε_0 is the vacuum dielectric constant and μ_0 is the permeability of vacuum.

The transmission coefficient t and reflection coefficient r of light can be expressed as

$$t = \left| \frac{2p_0}{(M_{11} + M_{12}p_t)p_0 + (M_{21} + M_{22}p_t)} \right| \tag{7}$$

$$r = \left| \frac{(M_{11} + M_{12}p_t)p_0 - (M_{21} + M_{22}p_t)}{(M_{11} + M_{12}p_t)p_0 + (M_{21} + M_{22}p_t)} \right| \tag{8}$$

where the subscripts "0" and "t" represent the incident and transmission space respectively. Therefore, the reflectance

R and transmittance T of the light absorber can be determined in the following ways:

$$R = |r|^2 \tag{9}$$

$$T = \frac{p_t}{p_0}|t|^2 \tag{10}$$

Therefore, the absorptivity of the optical absorber can be calculated by $A = 1$-R-T. As the bottom part of the designed absorber is containing a metal ground plane represented by a sliver substrate, the transmittance T is basically reduced to zero.

Simulations and Results

To explore the key features of the designed structure that are responsible for its effectiveness, we calculated the relationship between the absorption and several important structural parameters. One of them, D, is the thickness of the high refractive index TiO_2 layers D1 nd D2 located on the top of the upper and lower photonic crystals. It can be seen in Fig. 2a that with decreasing the thickness D, the TPP peaks have undergone relatively obvious blue shifts with substantially different slope ratios. As the absorptance of the resonance peak is relatively high when $D = 136$ nm, the thickness of the corresponding layer of the basic model structure is set to 136 nm. Figure 2b shows that as t_m, the thickness of the silver film increases, the positions of the three resonance peaks remain basically unchanged. $t_m = 27$ nm has been chosen as the default value when carrying out a variation analysis and topological optimization of the designing absorber.

Figure 3a shows a hybrid Tamm structure of the absorber with a graphene-based grating added onto the basic structure. The structure has two different types of resonance modes to achieve multiple absorption peaks, and the coupling effect of GMR and TPP modes on the improvement of absorption has been studied. In addition to enhancing the absorption of GMR peaks, the graphene monolayer, sandwiched between the grating and a dielectric layer of SiO_2, can increase the tunability of the structure. Here, we set the grating constant (also called the grating period) $P = 1.15$ μm, the thickness and width of the opaque part are $h = 0.4$ μm and $W = 0.25$ μm respectively, and the dielectric matching layer thickness $d = 1$ μm. Graphene monolayer thickness is determined at $t_g = 0.34$ nm with its dielectric permittivity $\varepsilon_g = 1 + i\sigma_g/(\omega\varepsilon_0 t_g)$, where σ_g is the surface conductivity of graphene and ε_0 is the vacuum dielectric constant; ω is the angular frequency of the incident wave. The conductivity is highly dependent on the chemical potential μ_c, which is determined at 0.3 eV in this work taking into account the data [32, 33]. The upper spectrum in Fig. 3b shows the absorptance when the resonance mode is excited by the TM polarization. For this structure, the graphene-based grating has little effect on the propagating light, which is almost equal to completely transmitting to the surface of the thin silver film of the Tamm structure. The spectrum shows three distinct TPP peaks with wavelengths of 1607 nm, 1684 nm, and 1785 nm, corresponding to three optical Tamm states, similar to those depicted in Fig. 1c. The lower spectrum in Fig. 3b resulted from the TE polarization excitation revealing a GMR peak at the wavelength of 1524 nm while keeping the same three OTSs, corresponding to the same three TPP resonance peaks. So this structure can be used for multichannel absorption filter devices, which can perfectly absorb incident light of four wavelengths at the same time to achieve a filtering effect. Figure 3c illustrates a Fabry Pérot (F-P) cavity resonance model, which has been proposed to understand the localization of the TPP resonances [34]. Because the one-dimensional PhC structure is relatively simple, it can be regarded as BR [13]. The excitation condition of the TPP mode generated at the interface of the BR and metal can be expressed as [5]:

$$r_M r_{BR} \exp(2i\delta) = 1 \tag{11}$$

Fig. 2 Spectral diagrams determine the absorptance peak positioning depending on **a** the thickness D and **b** t_m
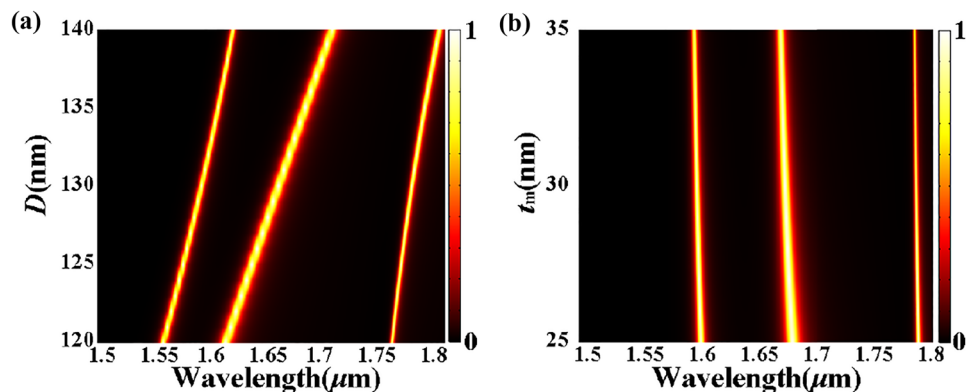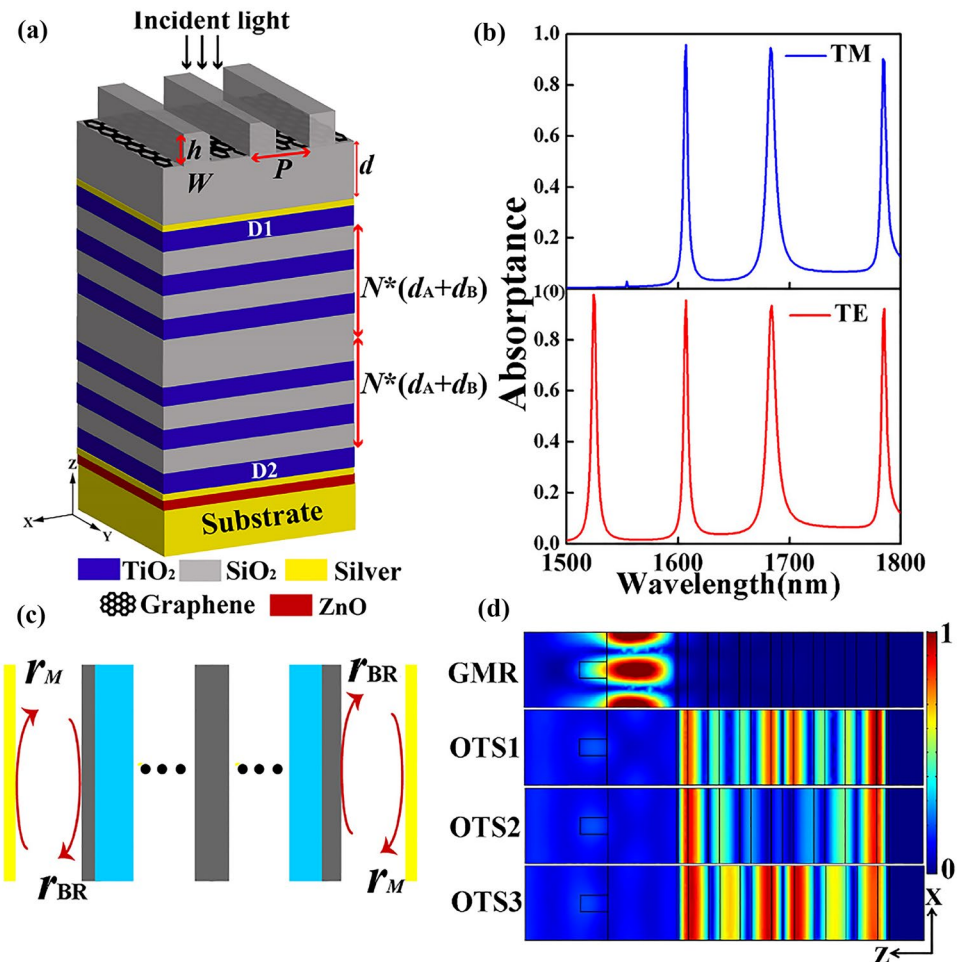
Fig. 3 **a** Three-dimensional schema of the multichannel absorption filter. **b** Absorption spectra when incident with TM and TE polarization respectively. **c** shows two identical cavities, both wrapped by silver films and BRs. **d** Electric field magnitude for the GMR and for three TPP modes when incident with TE polarization

where δ is the phase change between the interfaces, r_M represents the reflection coefficient for the wave incident on the silver layer from the BR, which can be obtained by the Fresnel formula, and r_{BR} is the reflection coefficient of the wave incident on the BR from the silver layer, which can be calculated by the transfer matrix method (TMM).

The resonance wavelength of the guided mode should meet the phase-matching condition [35, 36]:

$$k_{GMR} - k_0 \sin\theta = m\frac{2\pi}{P} \tag{12}$$

where $k_{GMR} = k_0 \cdot n_{eff}$ is the wave vector of the guided mode, n_{eff} represents the effective refractive index of the guided mode, m is the diffraction order, and $k_0 = 2\pi/\lambda$ is the wave number where λ is the incident wavelength. In particular, when $\theta = 0$ and $m = 1$, the above formula can be reduced to $\lambda_0 = n_{eff} \cdot P$. To better understand the GMR and TPP effects, the electric field distribution at the resonance is shown in Fig. 3d, from which it becomes clear that the GMR mainly occurs in the SiO_2 isolation layer, forming a typical standing wave profile. In other words, if the incident wave couples well with the leakage-guided mode, GMR will occur. At the
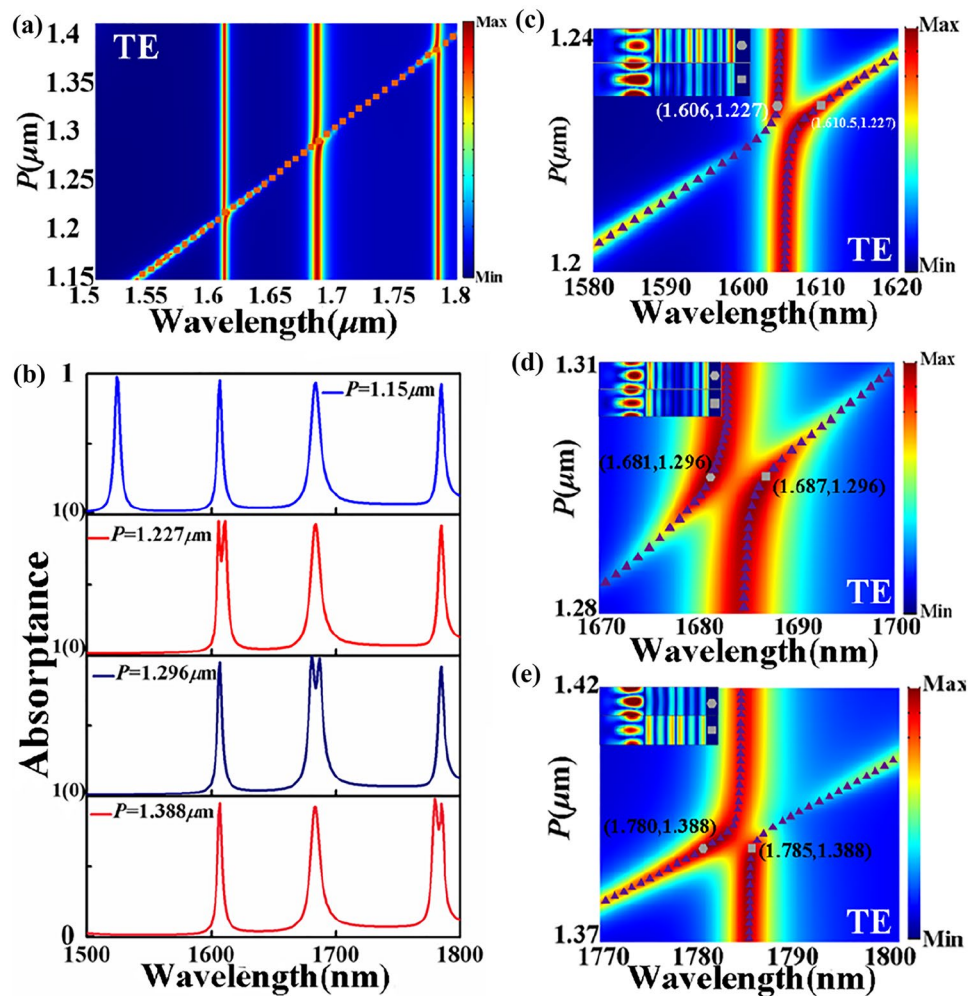
same time, it has been explained above that the TPP mode can be excited at the interface between the metal and the photonic crystal structure and between photonic crystals.

As shown in Fig. 4, changing the grating period length P will allow investigating the coupling effect between the GMR and TPP resonances depending on the wavelength and the polarization type (TE polarization). In Fig. 4a, the analytical results obtained using Eq. (12) and the results of numerical simulations are combined. As the P increases, the wavelength capable of exciting the GMR increases too, and at the corresponding P, the GMR couples with three TPP resonances. According to the classic two oscillator models, the frequency of the resonant mixed mode can be determined by [37–40]:

$$f_{\pm} = \frac{f_{GMR} + f_{TPP}}{2} \pm \frac{\sqrt{(f_{GMR} - f_{TPP})^2 + \Omega^2}}{2} \tag{13}$$

Here, $f_{\pm}$ is the resonance frequency of the hybrid modes, f_{GMR} and f_{TPP} represent the frequency of the GMR and the TPP resonance, and Ω is the interaction frequency between

Fig. 4 Evolution of absorption spectra of **a** the hybridized Tamm structure with the grating period length *P*, where the red square indicates the GMR. **b** Absorption spectrum at specific *P*; **c**, **d**, and **e** are enlarged views of the absorption spectra at the three resonance coupling locations. The insets show the enhanced electric field resonance of GMR and TPP at the locations marked by hexagons and squares

the two resonances. The dispersion relationship between GMR and TPP resonances can be calculated. The overlap between the two resonances occurs when varying the *P*. However, the two resonances will not impose exactly, but are separated by a small energy gap, exhibiting typical mode hybridization. The dotted curve marked by the purple triangles in Fig. 4c–e theoretically confirms the fact.

Figure 4b shows the absorptance spectrum at variable *P*, indicating that the GMR is capable of being hybridized with any of the three TPP resonances. It can be seen that the mode hybridization slightly increases the width of the absorption peak and the absorptance, which can be applied to the adjustment of the absorption filter in the narrow band. The split of curves visible in Fig. 4c–e and associated with

the resonance hybridization is called the Rabi split of the vacuum field [41–43]. It is necessary to note that the GMR and TPP resonances for all three cases are well described by theoretical approximation derived from Eq. 12 (dotted lines).

The GMR effectiveness is very sensitive to any variations with the chemical potential μ_c of the graphene grating, while the TPP resonances are irrelevant to the variations. In particular, when considering the 1524 nm resonance, the peak absorptance drops from 97.57 to 32.86% when μ_c increases from 0.4 to 0.42 eV, as shown in Fig. 5a and b. The polarization angle of the incident linearly polarized radiation is capable of influencing the GMR absorptance spectrum as it is shown in Fig. 5c and d, while the symmetry of the PhCs guarantees the independence of the TPP resonances on the polarization angle.
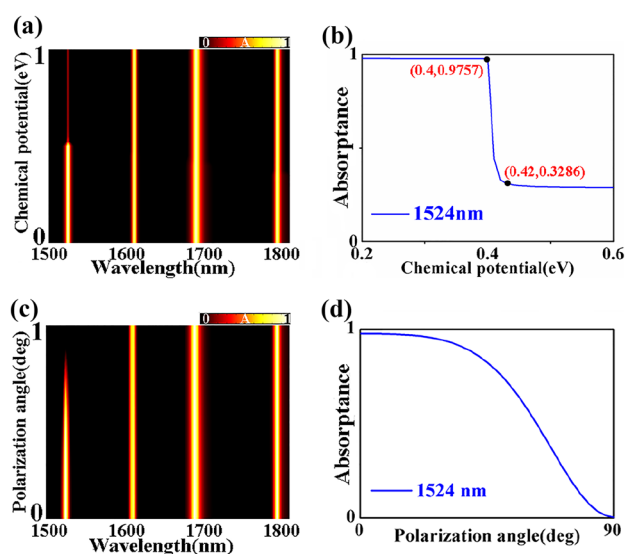
Fig. 5 a Spectral diagram representing the dependence of the absorption as a function of the wavelength and the chemical potential of graphene under TE polarization. **b** The dependence of absorptance versus chemical potential at 1524 nm. **c** Spectral diagram representing the dependence of the absorptance as a function of the wavelength and the polarization angle at normal incidence. **d** The dependence of absorptance versus chemical potential at 1524 nm

Conclusions

In general, the reason for the design of this structure is to explore the optical properties of the graphene-based grating combined with the double Tamm structure. Through simulation research, the structure can realize the tunable multichannel absorption effect and can be applied to the near-infrared optical filter. Using the TMM, CMT, and numerical simulations (COMSOL multiphysics), the results reveal that four remarkable absorption peaks are generated due to GMR and TPP. The grating period length variation facilitates the GMR relocation along with the spectra and superimposing with the TPP resonances, resulting in obvious mode hybridization. The silver thin film thicknesses used in the design of the absorber (M-PHC-M) can be varied without limiting the absorber's functionality. The positioning of the absorption peaks can be tuned by adjusting the thicknesses of the absorber's layers. In addition, the absorption filters can be used for selective polarization filtering of linearly polarized radiation, the throughput of which can be controlled by adjusting the chemical potential of graphene. The type of absorber can be potentially used as a part of optical devices such as sensors, modulators, switches, filters, and polarizers.

Declarations

Conflict of Interest The authors declare no competing interests.

References

1. Gao H, Li P, Yang S (2020) Tunable multichannel optical absorber based on coupling effects of optical Tamm states in metal-photonic crystal heterostructure-metal structure. Opt Commun 457:124688
2. Goto T, Dorofeenko AV, Merzlikin AM, Baryshev AV, Vinogradov AP, Inoue M, Lisyansky AA, Granovsky AB (2008) Optical Tamm states in one-dimensional magnetophotonic structures. Phys Rev Lett 101113902
3. Wang XY, Wang JC, Liu DD, Hu ZD, Zhang F (2018) Perfect absorption of molybdenum disulfide-based modified Tamm plasmonic structures. Appl Phys Express 11(6):062601
4. Kavokin AV, Shelykh IA, Malpuech G (2005) Lossless interface modes at the boundary between two periodic dielectric structures. Phys Rev B 72(23):3102
5. Kaliteevski M, Iorsh I, Brand S, Abram RA, Chamberlain JM, Kavokin AV, Shelykh IA (2007) Tamm plasmon-polaritons: possible electromagnetic states at the interface of a metal and a dielectric Bragg mirror. Phys Rev B Condens Matter 76(16):165415.1–165415.5

6. Sasin ME, Seisyan RP, Kalitteevski MA, Brand S, Abram RA, Chamberlain JM, Egorov AY, Vasil Ev AP, Mikhrin VS, Kavokin AV (2008) Tamm plasmon polaritons: slow and spatially compact light. Appl Phys Lett 92:251112

7. Vasily V, Klimov, Andrey A, Pavlov, Ilya V, Treshin, Ilya (2017) Fano resonances in a photonic crystal covered with a perforated gold film and its application to bio-sensing. J Phys D Appl Phys

8. Jiang X, Wang T, Zhong Q, Yan R, Huang X (2020) Ultrabroadband light absorption based on photonic topological transitions in hyperbolic metamaterials. Opt Express 28:705

9. Tsurimaki Y, Tong JK, Boriskin VN, Semenov A, Ayzatsky MI, Machekhin YP, Chen G, Boriskina SV (2017) Topological engineering of interfacial optical Tamm states for highly sensitive near-singular-phase optical detection. ACS Photonics 5:929–938

10. Pianelli A, Kowerdziej R, Dudek M, Sielezin K, Olifierczuk M, Parka J (2020) Graphene-based hyperbolic metamaterial as a switchable reflection modulator. Opt Express 28:6708

11. Shao H, Chen C, Wang J, Pan L, Sang T (2017) Metalenses based on the non-parallel double-slit arrays. J Phys D Appl Phys 50:384001

12. Yang L, Wang J, Yang L, Hu ZD, Wu X, Zheng G (2018) Characteristics of multiple Fano resonances in waveguide-coupled surface plasmon resonance sensors based on waveguide theory. Sci Rep 8:2560

13. Brand S, Kaliteevski MA, Abram RA (2009) Optical Tamm states above the bulk plasma frequency at a Bragg stack/metal interface. Phys Rev B: Condens Matter 79(8):85416–85416

14. Senanayake P, Hung CH, Shapiro J, Lin A, Liang B, Williams BS, Huffaker DL (2011) Surface plasmon-enhanced nanopillar photodetectors. Nano Lett 11:5279–5283

15. Afinogenov BI, Popkova AA, Bessonov VO, Fedyanin AA (2016) Measurements of the femtosecond relaxation dynamics of Tamm plasmon-polaritons. Appl Phys Lett 109:2349

16. Gazzano O, Vasconcellos SM de, Gauthron K, Symonds C, Bloch J, Voisin P, Bellessa J, Lemaitre A, Senellart P (2011) Full control of spontaneous emission in confined Tamm plasmon structures.

17. Zhang C, Wu K, Giannini V, Li X (2017) Planar hot-electron photodetection with Tamm plasmons. ACS Nano 11:1719–1727

18. Qing YM, Ma HF, Cui TJ (2019) Flexible control of light trapping and localization in a hybrid Tamm plasmonic system. Opt Lett 44:3302

19. Grigorenko AN, Polini M, Novoselov KS (2012) Graphene plasmonics. Nat Photonics 6(11):749–758

20. Jablan M, Buljan H, and Soljacic M (2009) Plasmonics in graphene at infrared frequencies. Physical Review 80(24): 245435.1–245435.7

21. Feng Y, Hu ZD, Wang JC, Balmakou A, Khakhomov S, Semchenko I, Liu DD, Sang T (2020) Perfect narrowband absorber based on patterned graphene-silica multilayer hyperbolic metamaterials. Plasmonics 15(6):1869–1874

22. Ju L, Geng BS, Horng J, Girit C, Martin M (2011) Graphene plasmonics for tunable terahertz metamaterials. Nat Nanotechnol 6(10):630–634

23. Ren Y, Guo X, Zhang G, Balakin AV, Shkurinov AP, Yu A, Zhu Y (2020) Excitation of graphene surface plasmons polaritons by guided-mode resonances with high efficiency. Opt Express 28:13224–13233

24. Wang JC, Yang L, Hu ZD, He WJ, Zheng GG (2019) Analysis of graphene-based multilayer comb-like absorption enhancement system based on multiple waveguide theory. IEEE Photonics Technol Lett 31(7):561–564

25. Hua LU, Gan X, Jia B, Mao D, Zhao AJ (2016) Tunable high-efficiency light absorption of monolayer graphene via Tamm plasmon polaritons. Opt Lett 41:4743–4746

26. Cheng HC, Kuo CY, Hung YJ, Chen KP, Jeng SC (2018) Liquid-crystal active Tamm-plasmon devices. Phys Rev Appl 9:64034

27. Wurdack M, Lundt N, Klaas K, Baumann V, Alexey V (2017) Observation of hybrid Tamm-plasmon exciton- polaritons with GaAs quantum wells and a MoSe2 monolayer. Nat Commun

28. Mischok A, Siegmund B, Ghosh DS, Benduhn J, Spoltore D, Bhm M, Frb H, Koerner C, Leo K, Vandewal K (2017) Controlling Tamm plasmons for organic narrowband near-infrared photodetectors. Acs Photonics 7b00427

29. Maji PS, Das R (2017) Hybrid-Tamm-plasmon-polariton based self-reference temperature sensor. J Lightwave Technol 35:2833–2839

30. Kumar S, Shukla MK, Maji PS, Das R (2017) Self-referenced refractive index sensing with hybrid-Tamm-plasmon-polariton modes in sub-wavelength analyte layers. J Phys D Appl Phys

31. Zhou H, Yang G, Wang K, Long H, Lu P (2010) Multiple optical Tamm states at a metal–dielectric mirror interface. Opt Lett 35:4112

32. Hu J, Qing Y, Yang S, Ren Y, Wu X, Gao W, Wu C (2017) Tailoring total absorption in a graphene monolayer covered subwavelength multilayer dielectric grating structure at near-infrared frequencies. J Opt Soc Am B 34:861

33. Dao TD, Ishii S, Doan AT, Wada Y, Ohi A, Nabatame T, Nagao T (2019) An on-chip quad-wavelength pyroelectric sensor for spectroscopic infrared sensing. Adv Sci 6:1900579

34. Zheng HY, Jin XR, Park JW, Lu YH, Rhee JY, Jang WH, Cheong H, Lee YP (2012) Tunable dual-band perfect absorbers based on extraordinary optical transmission and Fabry-Perot cavity resonance. Opt Express 20:24002–24009

35. Fu XY, Yi K, Shao JD, Fan ZX (2009) Design of single-material guided-mode resonance filter. Chin Opt Lett 7:9–11

36. Cai Y, Huang Y, Zhu K, Wu H (2019) Direction-independent dual-band perfect absorption induced by fundamental magnetic polaritons. Opt Express 27:A1431

37. Hu J, Yao E, Xie W, Liu W, Li D, Lu Y, Zhan Q (2019) Strong longitudinal coupling of Tamm plasmon polaritons in graphene/DBR/Ag hybrid structure. Opt Express 27:18642

38. Zhang D, Qiu D, Chen Y, Wang R, Zhu L, Wang P, Ming H, Badugu R, Stella U, Descrovi E (2019) Coupling of fluorophores in single nanoapertures with Tamm plasmon structures. J Phys Chem C

39. Nong J, Wei W, Wang W, Lan G, Shang Z, Yi J, Tang L (2018) Strong coherent coupling between graphene surface plasmons and anisotropic black phosphorus localized surface plasmons. Opt Express 26:1633

40. Hu T, Wang Y, Wu L, Zhang L, Shan Y, Lu J, Wang J, Luo S, Zhang Z, Liao L (2007) Strong coupling between Tamm plasmon polariton and two dimensional semiconductor excitons. Appl Phys Lett 110:51101

41. Wang JC, Wang XY, Hu ZD, Tang Y, Balmakou A, Khakhomov S, Liu D (2019) Independent tunable multi-band absorbers based on molybdenum disulfide metasurfaces. Phys Chem Chem Phys 21(43):24132–24138

42. Bao ZY, Wang JC, Hu ZD, Balmakou A, Zhang C (2019) Coordinated multi-band angle insensitive selection absorber based on graphene metamaterials. Opt Express 27:31435

43. Buzavaite-Verteliene E, Valavicius A, Grineviciute L, Tolenis T, Lukose NG, Balevicius Z (2020) Influence of the graphene layer on the strong coupling in the hybrid Tamm-plasmon polariton mode. Opt Express 28:10308–10319